Investigation of the Biodegradable Mechanism of Pure Magnesium Using Electrochemical Impedance Spectroscopy Technique

Woo-Cheol Kim[1], Seon-Hong Kim[1], Jung-Gu Kim[1,†], and Young-Yul Kim[2]

[1]Department of Advanced Materials Engineering, Sungkyunkwan University
300 Chunchun-Dong, Jangan-Gu, Suwon 440-746, Republic of Korea
[2]Department of Orthopaedics, Catholic University Sung-Mo Hospital, Daejeon 706-130, Republic of Korea

In this study, electrochemical impedance spectroscopy (EIS) was used to examine the changes in the electrochemical properties of biodegradable pure magnesium implanted into Sprague-Dawley rats for three days. The in vivo test results were compared with those of the in vitro tests carried out in Hank's, dilute saline and simulated body fluid (SBF) solutions. The in vitro corrosion rates were 20~1700 fold higher, as compared to the in vivo corrosion rates. This discrepancy is caused by biomolecule adsorption on the surface, which prevents the transport of water into the magnesium surface on in vivo testing. Among the in vitro experimental conditions, the corrosion rate in SBF solution had the least difference from the in vivo implanted specimen.

1. Introduction

Metallic implant materials are widely used for orthopedic bone implant materials. However, the elastic modulus of metallic biomaterial is much higher than that of natural bone and this mismatch causes stress shielding[1-6]. Furthermore, metallic biomaterials can release toxic ions and particles through corrosion or wearing processes to cause metal allergies, skin diseases and inflammatory cascades[1,4,7]. Moreover, a second surgical procedure is needed to remove the metal implant[1,2,8].

Recently, magnesium and magnesium alloy have attracted much attention as potential biodegradable materials in medical science because of their elastic modulus and compressive yield strength, their good biocompatibility and the promotion of new bone formation during the biodegradation process[9-11]. Due to these advantages, much research has been done for biodegradable orthopedic implants, vascular stents, and bone grafts[12,13]. However, the fast degradation limits their practical application[1,11,12].

Corrosion resistance is an important consideration in medical treatments requiring the implantation of metallic biomaterials in the human body[13]. The corrosion of metallic biomaterials used in orthopedic devices and other surgical implants can cause a range of problems, such as mechanical damage, hydrogen evolution and the formation of corrosion products[14-20]. Thus, evaluation of the corrosion resistance is very important for applications to metallic biomaterials.

Electrochemical and weight loss tests are widely used methods to study both in vivo and vitro corrosion properties of metallic biomaterials including magnesium and magnesium alloy. However, weight loss measurements are not sensitive enough and too difficult to apply the in vivo corrosion studies[14,15]. On the other hand, electrochemical methods are useful for in vivo measurements. These methods are not only very rapid and sensitive, but can also provide continuous measurements and measure the instantaneous corrosion rate of implanted specimens without removing them from the body[14,20]. Thus, in vivo electrochemical measurements provide a useful method for evaluating the corrosion resistance of metallic biomaterials. Normally, three kinds of simulated fluids are used in vitro test (dilute saline, Hank's, simulated body fluid (SBF) solutions)[21-23]. However, it is very difficult to simulate the in vivo environment because various organisms, such as bloodstream, proteins and cells, have complex interactions with each other inside the body. Actually, when a metal is implanted into body, the implant will be surrounded by muscle tissue, cells and proteins. Thus, the correlation between in vivo and in vitro allows prediction of the in

---

†Corresponding author: kimjg@skku.ac.kr

vivo corrosion performance of a biodegradable material based on its in vitro behavior[15].

In this paper, magnesium has been implanted into Sprague-Dawley (SD)-rat and three kinds of simulated fluids were selected to evaluate the difference of the in vivo and vitro electrochemical properties of magnesium. The investigated biodegradable mechanisms and optimized solution, which present closet characteristic as compared with the in vivo condition in this paper, could be useful for the research on the new biodegradable material. The biodegradable mechanism of in vivo and vitro environments was investigated by electrochemical impedance spectroscopy.

2. Experimental procedures

2.1. In vivo corrosion measurement

Commercially available pure magnesium (> 99.9 %) was used for in vivo and in vitro tests. Fig. 1 shows a schematic diagram of the in vivo test kit. A three-electrode EIS was used to evaluate the electrochemical properties of magnesium. The test specimen was cut into a rod of 2 mm in diameter and 10 mm in length. Copper wires were connected to the top of a working, counter and reference electrodes to establish an electrical connection. The specimen was ground with 600-grit SiC paper under moist condition. All surfaces, except for the exposed area (53.38 mm^2), were masked carefully with epoxy resin. A pure titanium and Ag/AgCl were used as the counter and the reference electrodes, respectively.

The animal studies were performed by Catholic University, Deajeon St. Mary's Hospital (Korea) to evaluate the deg-
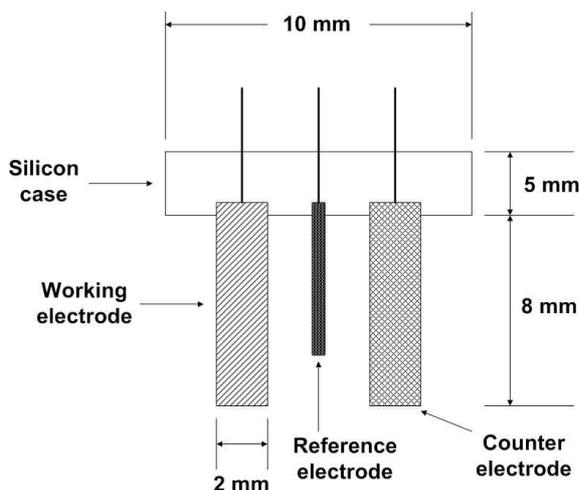
radation property. The experimental protocol was performed in accordance with local regulation (Korea animal welfare regulation) approved by the responsible animal care committee (Department of Laboratory Animal, IACUC, the Catholic University of Korea, CMCDJ-AP-2011-003). Twelve adult SD rats, 600 - 800 g in weight, were used in vivo experiments (Orient Bio, ChungBuk, Korea). The implant specimen was placed in the L5-6 disc space posteriorly. Animals were anesthetized with 6 mg/dl ketamine and 0.6 mg/dl lumpun with intra-abdominal injections. The posterior hair was removed with a shaver and cleaned with alcohol and betadine. A vertical incision was made and the muscle fascia was incised with a knife and retracted laterally to expose the posterior lamina and small transverse process. Using a curette, the inter-transverse ligament between laminae was removed and the posterior part of the spine was all exposed. Micro-drilling was then performed for decortications of cortical bone and the previously prepared implant specimen was placed in the L5-6 disc. Muscle fascia and skin were sutured with nylon. Daily EIS measurement was done with ketamine anesthesia and post surgical care were done for decreasing pain. Animals were

Table 1. Chemical composition of test solutions

Component	Hank's (g/L)	SBF (g/L)	Dilute saline (g/L)
NaCl	8.000	8.235	0.900
KCl	0.400	0.225	
NaHCO$_3$	0.350	0.355	
NaH$_2$PO$_4$H$_2$O	0.250		
Na$_2$HPO$_4$2H$_2$O	0.060		
MgCl$_2$	0.190		
MgSO$_4$7H$_2$O	0.060		
Glucose	1.000		
CaCl$_2$2H$_2$O	0.190		
K$_2$HPO$_4$3H$_2$O		0.231	
MgCl$_2$6H$_2$O		0.311	
1.0M ‑ HCl		39 mL	
CaCl$_2$		0.292	
Na$_2$SO$_4$		0.072	
Tris[hydroxymethyl] aminomethane buffer solution : TBS		6.118	

Fig. 1. Schematic diagram of the three-electrode test kit used in vivo tests.

sacrificed with CO_2 gas and posterior spine structures were collected at 3rd post operation day.

The corrosion rate was measured by EIS. The EIS instrumentation consisted of an EG&G Parstat 2263 and EIS software. The EIS measurement was obtained at open-circuit potential (OCP) with an amplitude of 30 mV in the frequency range from 100 kHz to 10 mHz. The experimental results were interpreted based on an equivalent circuit using a suitable fitting procedure elaborated by the ZSimpWin program.

2.2 In vitro corrosion measurement

The effect of the in vitro test solutions on the corrosion behavior was examined using EIS tests in Hank's solution, simulated body fluid (SBF) solution and dilute saline solution. Table 1 shows the chemical composition of each solution.

All experiments were carried out in 1000 mL (pH 7.4) solution at 37 ℃. The exposed area for the corrosion test was 1 cm². The cell contained a working electrode, a glass capillary probe connected to the reference electrode (saturated calomel electrode; SCE) and two graphite counter electrodes. The specimen was allowed to reach a stable open-circuit potential (OCP). One hour was needed for the OCP to stabilize within ± 5 mV. The test specimens were polished with 600-grit SiC paper. All surfaces except for the exposed area were masked carefully with epoxy resin.

2.3. Scanning electron microscopic observation.

Corrosion morphology and corrosion products were analyzed by a scanning electron microscopy (SEM) with an energy dispersive x-ray spectroscopy (EDS).

3. Results

3.1. In vivo corrosion measurements.

Fig. 2 shows the EIS test results for different time in vivo. The plots show two and three-time constant with time. Fig. 3 shows diagrams of the electrochemical equivalent circuits, which are prevalent circuits for Mg biodegradable material, used to interpret the EIS results for 3 days. The 1st day electrochemical equivalent circuit, two-time constant consisted of the solution resistance (R_s), interface capacitance between magnesium and the corrosion product (CPE2) and between the corrosion product and the solution (CPE1), as well as the layer resistance (R_{oxide}) of the corrosion product and charge transfer resistance (R_{ct}) on the substrate surface. After 2 days in the vivo test, three-time constant were necessary to fit the experimental data. The electrochemical equivalent circuit
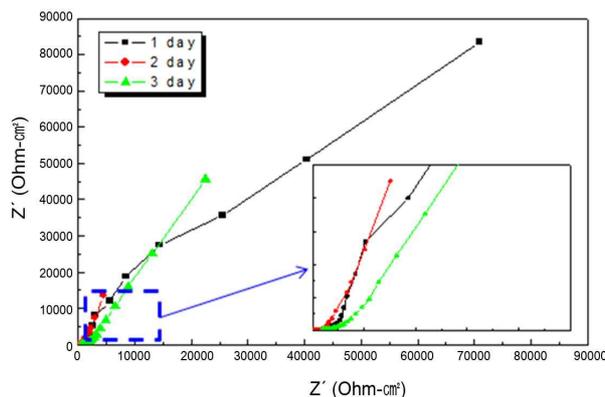

Fig. 2. Nyquist plot for the magnesium specimen in vivo environment.
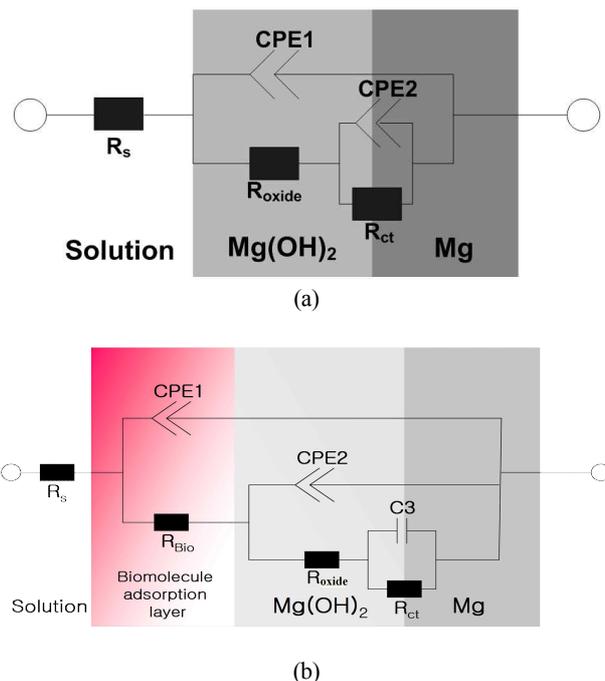

(a)

(b)

Fig. 3. Equivalent circuit used to fit the electrochemical impedance spectroscopy (EIS) diagram of the magnesium specimen in vivo environment: (a) 1 day of implantation and (b) after 2 and 3 days of implantation.

during the 2nd to 3rd days included a biomolecule adsorption layer[24]. Fig. 4(a) shows the biomolecule adsorption layer resistance with time. The resistance of biomolecule adsorption layer increased with implant time during 2nd to 3rd days. Fig. 4(b), (c) shows the change of oxide layer and charge transfer resistance. The value of the 1st day oxide layer resistance was higher than that of 2nd and 3rd days. Also, the highest charge transfer resistance was observed on the 1st day. The value of charge transfer resistance was decreased with time. Fig. 5 shows the corrosion
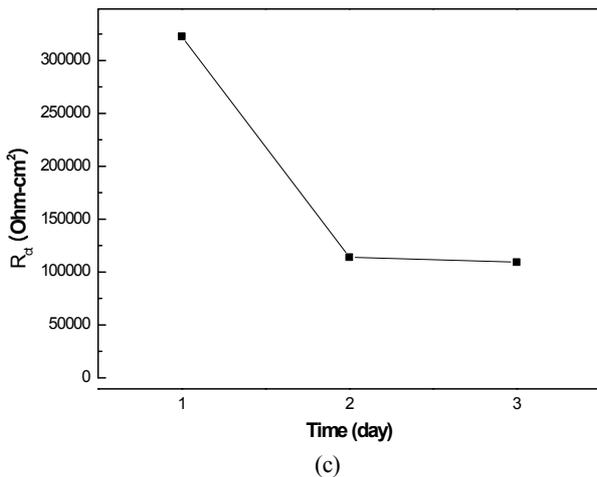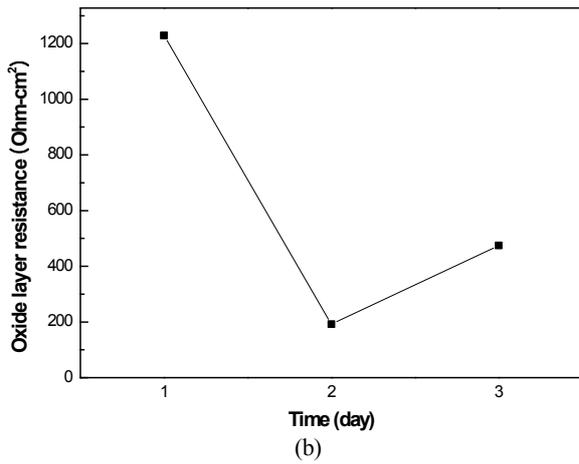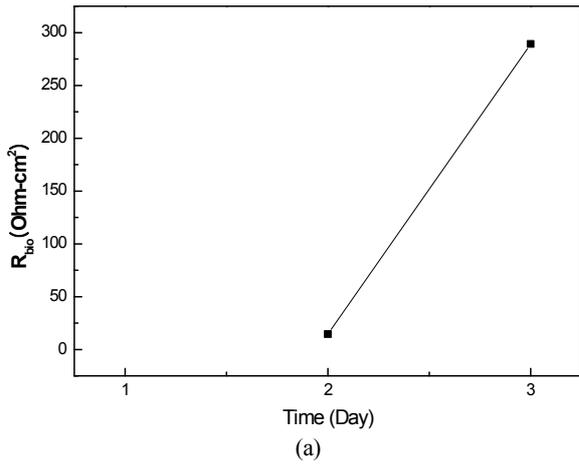
(a)

(b)

(c)

Fig. 4. Changes in the impedance of in vivo specimen: (a) bio-molecule adsorption layer resistance; (b) oxide layer resistance and (c) charge transfer resistance.

rate as a function of time for the in vivo testing. Corrosion rate was determined by polarization resistance R_p ($R_p = R_{oxide} + R_{ct}$). The lowest corrosion rate was observed on
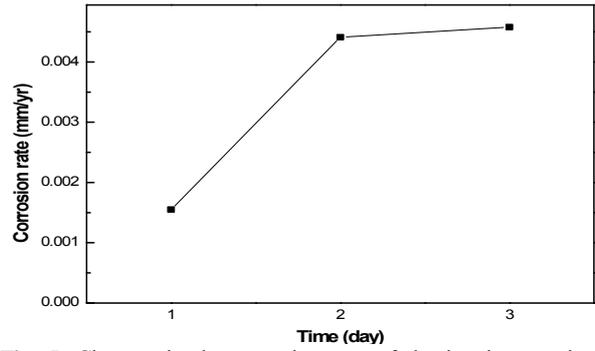

Fig. 5. Changes in the corrosion rate of the in vivo specimen.
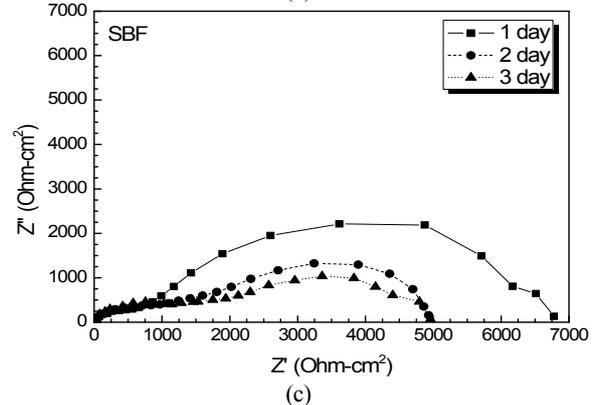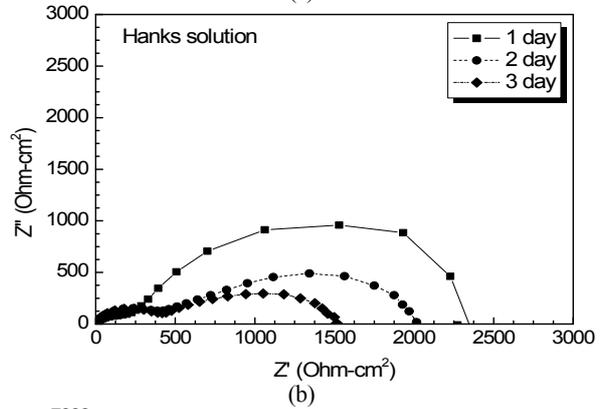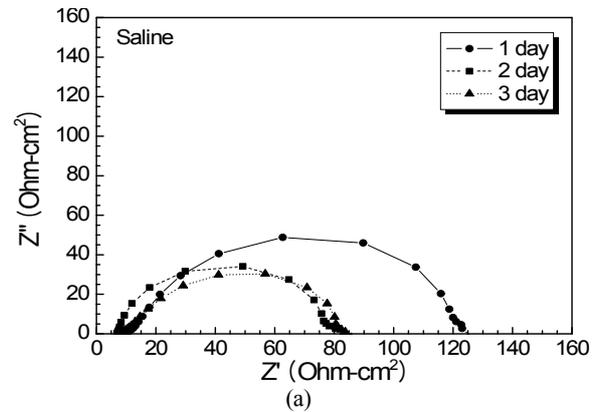

(a)

(b)

(c)

Fig. 6. Nyquist plot for the magnesium specimens in vitro environment: (a) Saline solution; (b) Hank's solution and (c) SBF solution.
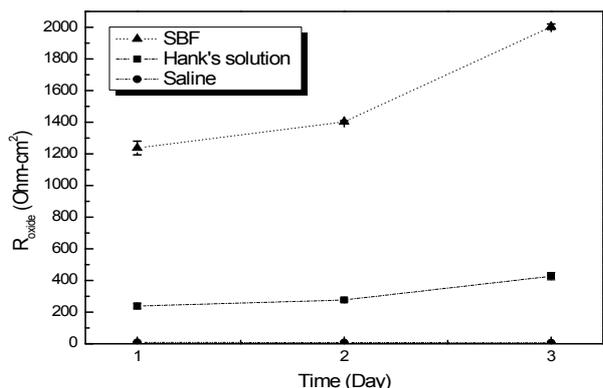
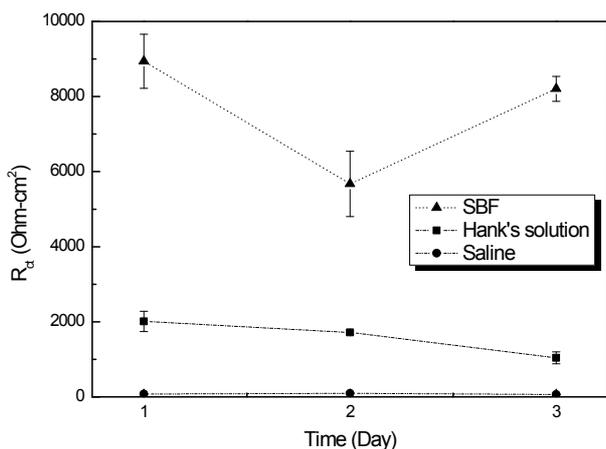**Fig. 7.** Changes in the impedance of the oxide layer on the in vitro specimens.

Fig. 8. Changes in the impedance of the charge transfer resistance on the in vitro specimens.
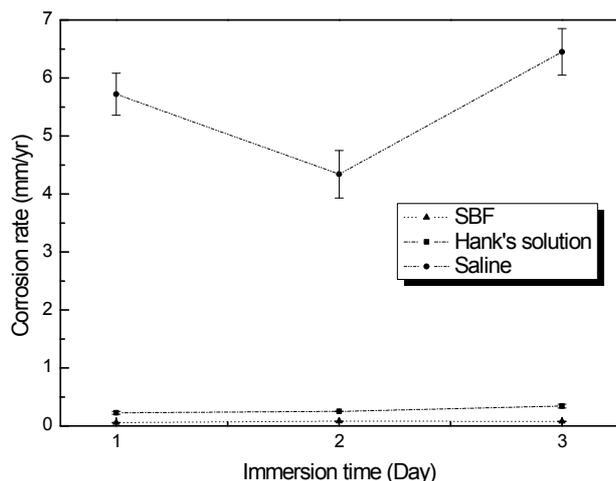

**Fig. 9.** Changes in the corrosion rate of the in vitro specimens.

the 1st day, which then increased with increasing implant time.

3.2. In vitro corrosion measurements

Fig. 6 shows the impedance spectra of in vitro shown up to two-time constant for three-day exposure. The electrochemical equivalent circuit of the in vitro was equal to that of the 1st day of in vivo test. Three solutions were investigated: dilute saline, Hank's and simulated body fluid solutions. Fig. 7 shows that the impedance of the oxide layer increased with increasing immersion time in all of the solutions and that SBF achieved the highest impedance during the test. Fig. 8 shows variation of the charge transfer resistance with time. The SBF achieved the highest impedance during the test.

Fig. 9 shows the change in corrosion rate as a function of the immersion time. SBF achieved the lowest corrosion rate during the test.

Generally, pH of neutral electrolyte involving solid magnesium was increased by cathodic reaction on the electrode surface. Moreover, stabilization of protective layer by the increase in the pH ultimately decreases the corrosion rate of magnesium. However, R. Lindström et al[24] suggested the decrease in pH by carbonic acid in ambient CO_2 environment.

$$CO_2(aq) + H_2O \leftrightarrow HCO_3^{3-} + H^+ \tag{1}$$

$$HCO_3^- \leftrightarrow CO_3^{2-} + H^+ \tag{2}$$
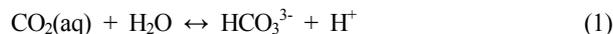
Therefore, corrosion rate was not increased with increasing immersion time in Fig. 9 because an increase in pH by the hydroxide is counteracted by the decreased in pH by carbonic acid.

Table 2 lists the average corrosion rates of magnesium in vivo and in vitro tests. There are noticeable differences between the in vivo and in vitro corrosion tests. The corrosion rate in SBF solution was lower than those in the dilute saline and Hank's solution. Moreover, SBF produced a more comparable result to the in vivo test than the other solutions. However, corrosion rate achieved from in vivo test was approximately 1 ~ 3 orders of magnitude lower than those achieved from in vitro tests.

Table 2. Corrosion rate of magnesium determined from the EIS test under in vitro and in vivo conditions

Solution	In vitro			In vivo
	Saline	Hank's	SBF	
Corrosion rate (mm/y)	5.96 ±0.4	4.03×10^{-1} ±0.03	7.14×10^{-2} ±0.004	3.51×10^{-3}
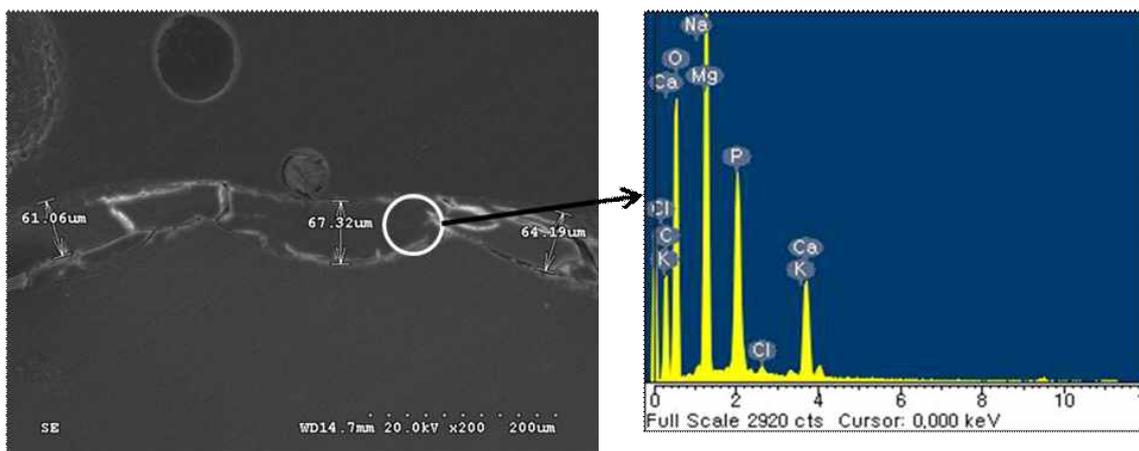
Element	Wt%	At%
C	29.80	40.13
O	44.98	45.48
Na	0.28	0.19
Mg	12.60	8.38
P	6.84	3.57
CI	0.27	0.12
K	0.21	0.09
Ca	5.02	2.02

Fig. 10. SEM cross-sectional image and EDS spectra of the in vivo specimen.

3.3 Scanning electron microscopic observation

After a 3-day implantation, the corrosion products were examined by SEM and EDS. Fig. 10 shows SEM cross-sectional image of the in vivo specimen along with the EDS result. The oxide layer was formed on the magnesium. The 60 μm oxide layer consisted of Mg, O, C, Ca and P. It confirms the formation of calcium phosphate on the surface in vivo.

Fig. 11 shows a SEM cross-sectional image and EDS spectra of the in vitro specimen. The thickness of the oxide layers formed in the Hank's and SBF solutions were approximately 5 μm and 14 μm, respectively with the products consisting of Mg, O, C, Ca, and P. The thickness of the oxide layer formed in the dilute saline solution was approximately 30 μm and the product consisted of Mg and O. This result confirmed that the oxide layers formed in Hank's and SBF solutions were consisted of calcium phosphate.
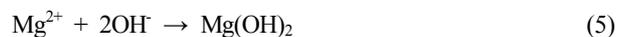
4. Discussion

Fig. 12 shows a schematic diagram of the major processes that occur at the magnesium surface under vitro environments. The magnesium in vitro environment dissolves according to the following reactions[25]:

Anodic reaction:
$$Mg \rightarrow Mg^{2+} + 2e \qquad (3)$$

Cathodic reaction:
$$2H_2O + 2e \rightarrow H_2 + 2OH^- \qquad (4)$$

$$Mg^{2+} + 2OH^- \rightarrow Mg(OH)_2 \qquad (5)$$

In general, the corrosion properties of magnesium are enhanced by $Mg(OH)_2$ [26]. For $Mg(OH)_2$, the protection property increased with increasing solution pH but can be destroyed by Cl^- ions[27-28]. However, the present study showed an opposite result. From Table 1, the concentration of Cl^- ions in the solutions was in the following order: SBF > Hank's > dilute saline, whereas the oxide layer resistance was SBF > Hank's > dilute saline in Fig. 7.

According to Y. Wang et al.[12], Ca and P accumulate inside porous $Mg(OH)_2$, which is formed during the early stages of corrosion, and may act as a barriers against the upcoming permeations. Also, N. T. Kirland et al.[29], re-
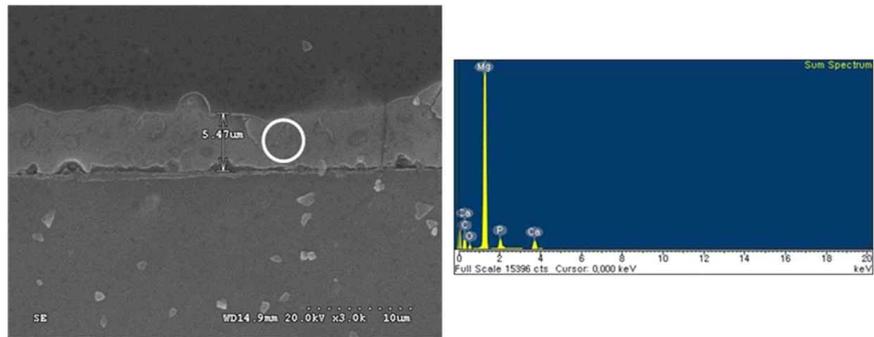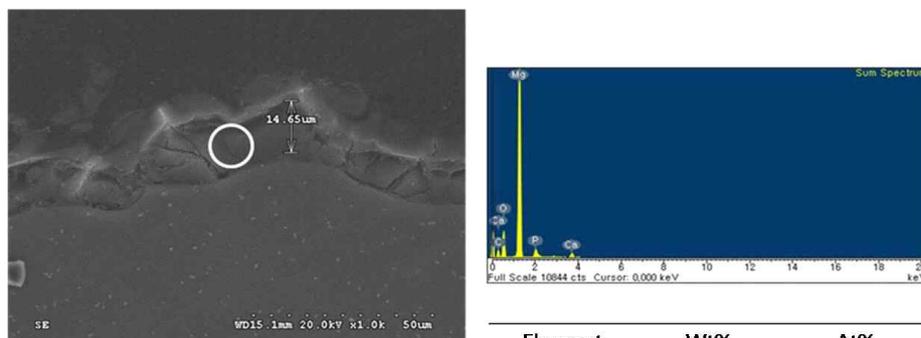
Element	Wt%	At%
C	43.88	60.44
O	8.07	8.34
Mg	41.12	27.98
P	3.15	1.68
Ca	3.77	1.56

(a)
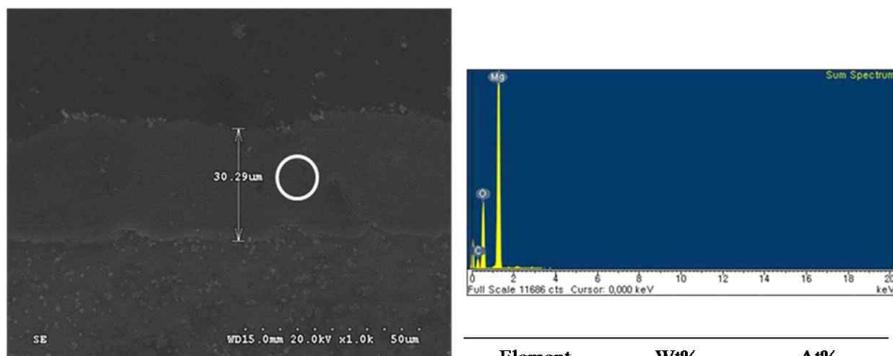
Element	Wt%	At%
C K	18.44	26.41
O K	43.15	46.40
Mg K	38.41	27.18

(b)

Element	Wt%	At%
C K	20.63	30.88
O K	29.75	33.43
Mg K	44.99	33.27
P K	2.63	1.53
Ca K	2.00	0.90

(c)

Fig. 11. SEM cross-sectional image and EDS spectra of the in vitro specimens: (a) Hank's solution; (b) Saline solution and (c) SBF solution.
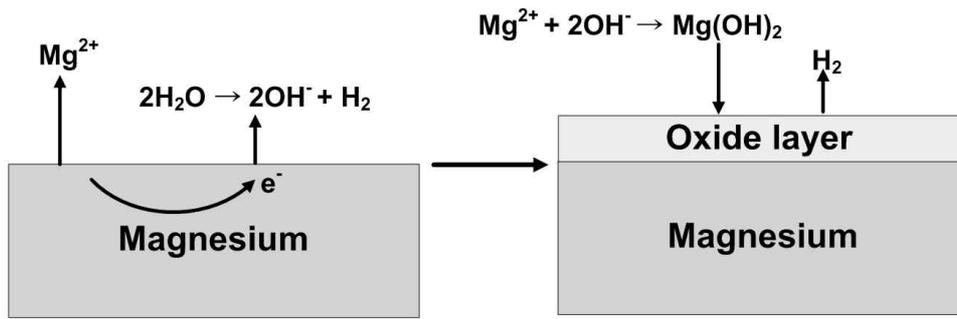
Fig. 12. Schematic illustration of reactions between magnesium and environment in vitro.
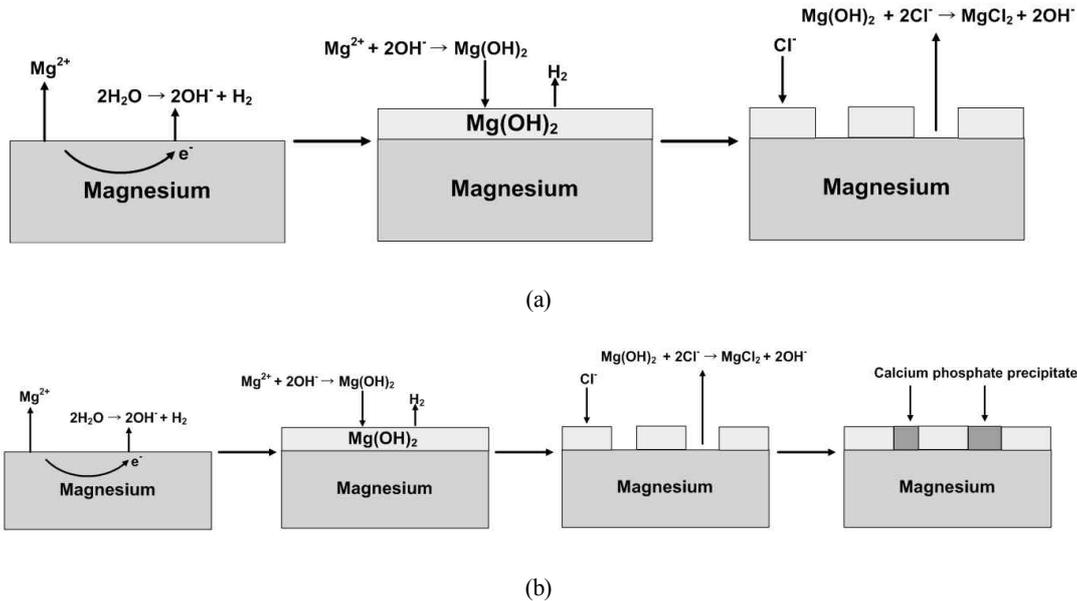

(a)

(b)

Fig. 13. Schematic illustration of the corrosion mechanism of magnesium in vitro environment: (a) saline solution; (b) Hank's and SBF solution.

ported that the another potential reason for the decrease of corrosion rate of magnesium is the formation of a calcium carbonate (CaCO$_3$) or magnesium carbonate (MgCO$_3$) layer on the surface. Calcium salts, such as CaCO$_3$ and CaP, are known to be cathodic inhibitors of corrosion for metals.

Fig. 13 shows a schematic diagram of the mechanism for the improvement in oxide layer resistance by calcium phosphate. The protection property in the oxide layer increased with time due to the increasing pH according to the cathodic reaction (4).

The results confirmed that the oxide layer resistance of a specimen immersed in Hank's solution and SBF solution, where calcium phosphate[23] formed, was higher than the specimen in the dilute saline solution without calcium phosphate formation. Also, oxide layer resistance was influenced by its thickness. From Fig. 8 and 11, the resist-

ance of the oxide layer increased with increasing its thickness in SBF and Hank's solutions and that SBF achieved the highest resistance. This result indicated that the oxide layer resistance was affected by formation of calcium phosphate and thickness (formation of calcium phosphate > thickness). Therefore, the resistance of the oxide layer on magnesium in vitro test solution was influenced more by the formation of calcium phosphate and thickness than by the concentration of Cl$^-$ ions in solution.

However, the in vivo experiments showed a different result from the in vitro one. When the specimen was implanted into the rat body (in vivo environment), biological factors, such as cells and proteins, became attached to the specimen surface. These biological factors cause the differences between the in vivo and vitro environments[30-32]. Fig. 14 shows a schematic diagram of the major processes that occur at the magnesium surface under in vivo environment.
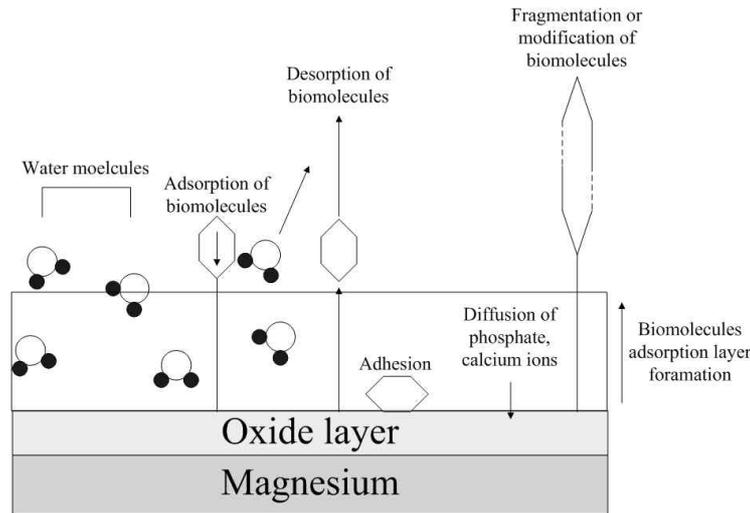
Fig. 14. Schematic illustration of reactions between magnesium and environment: in vivo.
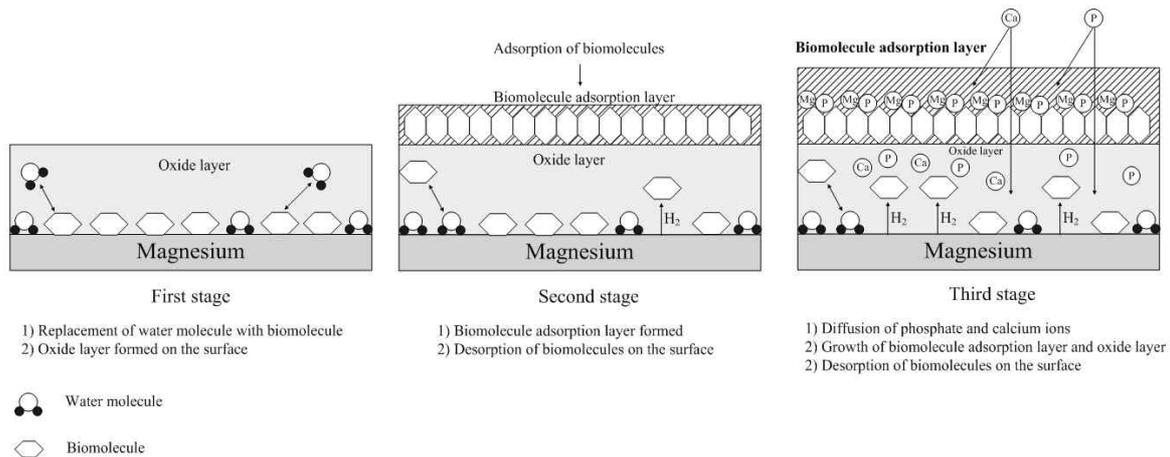

Fig. 15. Schematic diagram of the corrosion mechanism under in vivo environment.

This phenomenon can be explained by the electrochemical equivalent circuit in this study.

As shown in Fig. 3, the equivalent circuit consisted of magnesium, the basic material and Mg(OH)$_2$, as the corrosion product. The corrosion resistance in vivo condition was much higher than in vitro conditions. Under in vivo condition, a biomolecule adsorption layer[32] that was not present under the in vitro condition should have formed. Biomolecule-containing layer would be formed, inhibiting the contact between electrolyte and magnesium surface, therefore reducing the further corrosion[33,34]. Fig. 4(a) shows that the impedance of the biomolecule adsorption layer increased with increasing implant time on the 2nd to 3rd days. However, the resistance of the oxide layer decreased on the 2nd day and then increased on the 3rd day. The decrease in oxide layer resistance after the 2nd day was attributed to interactions between the proteins and

oxide after the proteins had been absorbed in the oxide layer.[31] In addition, calcium phosphate was detected in the oxide layer, suggesting that the increase in resistance on the 3rd day was due to the formation of calcium phosphate. The development of biomolecules adsorption layer was facilitated by the production of extracellular polymeric substances (EPS) comprising macromolecules (e.g. protein, polysaccharides, nucleic acid, lipids). Metal binding by EPS involves interaction between the ions and anionic functional groups such as phosphate, sulfate, glycerate. Especially the affinity of multidentate anionic ligands for multivalent ions, such as Ca^{2+}, Mg^{2+}, Cu^{2+}, Fe^{3+}, can be very strong[35]. Therefore, more thick oxide layer was formed on the surface in vivo than that of vitro one. However, biomolecules adsorption layer and oxide layer resistance in vivo is similar to oxide layer resistance in vitro. Therefore, that is not critical factor for determin-

ing the corrosion rate.

Fig. 4(c) shows the charge transfer resistance in vivo. The charge transfer resistance in vivo test was as much as 10 ~ 1000 times higher than that in vitro test. This suggests that the charge transfer resistance is a critical factor determining the corrosion rate.

A conducting metal immersed in an aqueous solution forms a complex interface known as the Helmholtz plane via an interaction between the metal surface and H_2O molecules. This plane prevents the close approach of charged species (ion) from the bulk solution[36]. However, the nature of the proteins involved in vivo environment results in the replacement of water molecules with bio-molecules[37]. This phenomenon often leads to a rearrange-ment of charged groups. Biomolecules adsorbed on the surface, prevented the diffusion of water molecules to the surface. Hence, the rate of the cathodic reaction of magne-sium was reduced and the charge transfer resistance of in vivo was higher than that of in vitro results. However, magnesium generates the hydrogen gas on the surface by cathodic reaction and it may lead to desorption of bio-molecule on the magnesium surface. Therefore, charge transfer resistance decreased with implanted time. Fig. 14 shows a schematic diagram of the corrosion processes that occur at the magnesium surface under in vivo environment.

The corrosion of metals is greatly affected by the surroundings. Therefore, to carry out a precise test, it is essential to set the conditions to be closest to the real one. F. Witte[15] suggested that the differences between the in vivo and in vitro tests are affected by pitting corrosion induced by ions, such as Cl^-. However, the present study showed that the formation of calcium phosphate has a more significant effect than Cl^-. Moreover, the differences between the in vivo and in vitro experiments were attrib-uted to the adsorption of biomolecules on the surface and the interaction between magnesium and biological factors, such as proteins.

5. Conclusions

This paper examined the effects of in vivo and in vitro environments (Hank's, SBF, saline) on the corrosion rates of biodegradable magnesium using EIS. The corrosion rate of the in vitro specimen was as much as 20 ~ 1700 times higher than that in vivo specimen. The performance of the rust layer on the magnesium in vitro environment was affected more by the formation of calcium phosphate than by the amount of Cl^- ions in solution. Also, charge transfer resistance was found to be a critical factor for determining the corrosion rate and was affected by the adsorption of biomolecules on the surface. Biomolecules, such as pro-

teins and cells, are the main reason for the difference be-tween the in vivo and vitro environments. Therefore, it is important to consider the biomolecules present under in vivo condition when performing an in vitro test.

References

1. M. P. Staiger, A. M. Pietak, J. Huadmai, G. Dias, *Biomaterials,* **27**, 1728 (2006).
2. J. Y. Lee, G. S. Han, Y. C. Kim, J. Y. Byun, J. I. Jang, H. K. Seok S. J. Yang, *Met. Mater. Int.*, **1,** 955 (2009).
3. F. Witte, N. Hort, C. Vogt, S. Cohen, K. U. Kainer, R. Willumeit, F. Feyerabend, *Curr. Opin. Solid State Mater. Sci.,* **12**, 63 (2008).
4. E. Zhang, L. Xu, G. Yu, F. Pan, K. Yang, *J. Biomed. Mater. Res. A,* **90A**, 882 (2009).
5. D. R. Sumner, J. O. Galante, *Clin. Orhop. Relat. Res.,* **274**, 202 (1992).
6. J. Nagels, M. Stokdijk, P. M. Rozing, *J. Shoulder Elb. Surg.,* **12**, 35 (2003).
7. D. A. Puleo, W. W. Huh, *J. Appl. Biomater.,* **6**, 109 (1995).
8. G. Mani, M. D. Feldman, D. Patel, C. M. Agrawal, *Biomaterials,* **28**, 1689 (2007).
9. Z. Li, X. Gu, S. Lou, Y. Zheng, *Biomaterials*, **29**, 1329 (2008).
10. L. Xu, F. Pan, G. Yu, L. Yang, E. Zhang, K. Y. Yang, *Biomaterials*, **30** 1512 (2009).
11. W. D. Mueller, M. L. Nascimento, M. F. Lorenzo, *Acta Biomater.*, **6**, 1749 (2010).
12. Y. Wang, M. Wei, J. Gao, J. Hu, Y. Zhang, *Mater. Lett.*, **62**, 2081 (2008).
13. V. J. Colangelo, N. D. Greene, *J. Biomed. Mater. Res.,* **1**, 405 (1967).
14. M. G. Fontana, N. D. Greene, *Corrosion Engineering*, p. 390, McGraw-Hill, New York (1978).
15. F. Witte, J. Fischer, J. Nellesen, H. A. Crostack, V. Kaese, A. Pisch, F. Beckmann, H. Windhagen, *Biomaterials*, **27**, 1013 (2006).
16. E. D. McBride, *J. Am. Med. Assoc.*, **27**, 2464 (1938).
17. J. Verbrugge, *La. Press. Med.*, **23**, 460 (1934).
18. J. T, Scales, G. D. Winter, *J. Bone Joint Surg.*, **41-B**, 810 (1959).
19. J. Cohen, J. Wulff, *J. Bone Joint Surg.*, **54-A**, 617 (1972).
20. N. Yuichiro, Y. Takao, K. Yosihiko, O. Masanori, *Biomaterials*, **10**, 420 (1989).
21. S. R. Sousa, M. A. Barbosa, *Clin. Mater.*, **14**, 287 (1993).
22. W. C. Kim, J. G. Kim, J. Y. Lee, H. K. Seok, *Mater. Lett.*, **62**, 4146 (2008).
23. K. Tadashi, T. Hiroaki, *Biomaterials,* **27**, 2907 (2006).
24. R. Lindström, L. Johansson, G. E. Thompson, P. Skeldon, J. Svensson, *Corros. Sci.*, **46**, 1141 (2004).

25. S. Zhang, X. Zhang, C. Zhao, J. Li, Y. Song, C. Xie, H. Tao, Y. Zhang, T. He, Y. Jiang, Y. Bian, *Acta Biomater.*, **6**, 626 (2010).
26. P. Schmutz, V. Guillaumin, R. S. Lillard, J. A. Lillard, G. S. Frankel, *J. Electrochem. Soc.*, **150**, B99 (2003).
27. G. Williams, H. N. McMurray, *J. Electrochem. Soc.*, **155**, C340 (2008).
28. G. L. Song, A. Atrens, *Adv. Eng. Mater.*, **1**, 11 (1999).
29. N. T. Kirkland, J. Waterman, N. Birbilis, G. Dias, T. B. F. Woodfield, R. M. Hartshorn, M. P. Staiger, *J. Mater. Sci. Mater. M.,* **23**, 283 (2012).
30. M. Browne, J. Gregson, *Biomaterials,* **15**, 894 (1994).
31. J. A. Helsen, H. J. Breme, *Metals as Biomaterials*, p. 102, John Willey & Sons New York (1998).
32. S. Hiromoto, K. Noda, T. Hanawa, *Corros. Sci.*, **44**, 955 (2002).
33. C. Liu, Y. Xin, X. Tian, P. K. Chu, *J. Mater. Res.*, **22**, 1806 (2007).
34. C. Liu, Y. J. Wang, R. C. Zeng, X. M. Zhang, W. J. Huang, P. K. Chu, *Corros. Sci.*, **52**, 3341 (2010).
35. I. B. Beech, J. Sunner, *Curr. Opin. Biotech.*, **15**, 181 (2004).
36. D. A. Jones, *Principles and Prevention of Corrosion*, 2nd *ed.*, p. 40, Prentice-Hall, NJ (1996).
37. J. A. Helsen, H. J. Breme, *Metals as Biomaterials*, p. 186, John Willey & Sons New York (1998).